Materials Characterization 191 (2022) 112128

Contents lists available at ScienceDirect

Materials Characterization

journal homepage: www.elsevier.com/locate/matchar

High-quality dissimilar friction stir welding of Al to steel with no contacting between tool and steel plate

M. Zhang [a,b], Y.D. Wang [a,b], P. Xue [a,b,*], H. Zhang [a,b], D.R. Ni [a,b,*], K.S. Wang [c], Z.Y. Ma [a,b]

[a] Shi-changxu Innovation Center for Advanced Materials, Institute of Metal Research, Chinese Academy of Sciences, Shenyang 110016, China
[b] School of Materials Science and Engineering, University of Science and Technology of China, Shenyang 110016, China
[c] School of Metallurgical Engineering, Xi'an University of Architecture and Technology, Xi'an 710055, China

ARTICLE INFO

Keywords:
Friction stir welding
Dissimilar joint
Thickness difference
Interface
Intermetallic compound

ABSTRACT

The stirring tools made of steels are easily worn in traditional friction stir welding (FSW) of Al alloy to steels, which limits their wide application in industry. Here, we reported a new FSW method with no contacting between the tool and the steel plate, and an ordinary H13 steel tool can be used in this case. In this study, thickened Al alloy plate was applied during FSW of 1060Al to SUS304 stainless steel. The results showed that a high-quality joint was successfully acquired at an appropriate thickness difference of 0.7 mm between Al and steel plates, where an excellent metallurgical bonding achieved in the Al-steel interface. Microstructure characterization revealed a thin interface layer (< 1 μm) consisted of Al_5Fe_2 intermetallic compound (IMC) and $Al_{13}Fe_4$ IMC as well as Al-based solid solution with enrichment of Ni. The joint failed at the heat affected zone of Al side with a high strength of 104 MPa (95% of 1060Al). This study brings a low-cost and effective method in FSW of Al alloy and high fusion-point metals, and can realize long-distance and high-quality welding in industry.

1. Introduction

The effective combination of Al alloy and steel will promote structural lightweight and functionality optimization in various transportation systems, due to the extensive and intersecting application of these two materials [1–3]. However, it is a big challenge to obtain Al-steel bimetallic structures through conventional fusion welding techniques due to their huge differences in physical and chemical properties [4,5]. Solid-state welding of Al alloy to steel, in particular, friction stir welding (FSW) shows great potential in avoiding defects caused by fusion welding on account of its low heat input and has successfully aroused considerable interest in recent years [6–8].

During the conventional FSW of Al alloy to steel, the stiring tool should possess very high performance because it needs to be inserted into the hard steel plates. In this case, several extraordinary materials such as polycrystalline cubic boron nitride (PCBN) [9,10], tungsten-rhenium (W—Re) alloy [11], and tungsten carbide [7,12,13] have been used owing to their high strength and hardness. However, considering both the material and machining costs as well as the chemical properties, these tools are unlikely to be widely exploited in industrial application [14]. For example, Park et al. [9] found that the formation of borides increased the susceptibility to pitting in the weld during FSW of austenitic stainless steels while using the PCBN tool. Considering the advantages of cost-effectiveness and reusability, steel is often preferred as an ideal tool material in FSW of Al alloys. However, it is difficult to apply in butt welding of hard and high fusion-point alloys (steel, Ti alloy, etc.), and the dissimilar joints between them and Al alloys.

In addition to tool material selection, tool position is also noteworthy in the application of Al-steel butting welding. When the steel tool was inserted into the center of the Al-steel interface, the joint was prone to failure due to inadequate material stirring caused by the rapid wear or fracture of the pin [15]. On the other hand, it is also believed that a great part of the tool into the steel side gave rise to excessive heat input, thus increasing the likelihood of forming intermetallic compounds (IMCs) and defects [16]. To avoid the above-mentioned issues, some researchers incline to set a tool offset towards Al alloy for a certain distance so that the surface quality and joint strength can be improved [12,17]. Nevertheless, the tool is still subjected to severe stress because the shoulder and pin of the tool have contact with the steel. In addition, there are many large-scale steel fragments scattered in the Al matrix owing to the intense stirring effect, which can result in abnormal material flow and the formation of void defects [15].

When the pin is completely offset to the Al alloy, the size of steel fragments in the Al matrix becomes small and the number is reduced

* Corresponding authors.
E-mail addresses: pxue@imr.ac.cn (P. Xue), drni@imr.ac.cn (D.R. Ni).

https://doi.org/10.1016/j.matchar.2022.112128
Received 20 March 2022; Received in revised form 22 June 2022; Accepted 13 July 2022
Available online 16 July 2022

clearly, but the joint strength is not optimistic. It is reported that the maximum tensile strength of the joint was only 36% of that of 5083Al when the pin just contacted with the steel faying surface [15]. Obviously, the heat generation is not sufficient to produce an effective metallurgical bonding under the condition. Furthermore, even if the pin is away from the steel, the tool shoulder is still in contact with the steel plate in the previous Al-steel FSW with equal-thickness plates. In this case, realizing long-distance welding will be a huge challenge. It is reported that the method of no contact of tool with steel has been used in the friction stir lap welding (FSLW) [18] and friction stirring spot welding (FSSW) [19,20] of Al to steel. According to the literature available, the pin was maintained above the surface of the lower steel sheet to avoid the rapid wear of the pin, where an effective bonding between Al and steel could be promoted by an indirect diffusion joining mechanism under sufcient heat and pressure.

Based on the aforementioned factors, no contacting with the steel plate is the precondition to use the most practical steel tool during FSW of Al-steel. Howerver, insufficient heat generation will be the key factor relating to the Al-steel metallurgical bonding and weld formation. Actually, increasing the thickness of Al alloy is a simple and effective method to solve the above problem. When the thickness of Al alloy plate is larger than that of the steel plate, both the shoulder and the pin of the tool can not contact with the steel plate. Further, due to the large plunge depth of the shoulder into the Al alloy, enhanced forge force and friction heat will be achieved during FSW. In this case, good weld formation can be obtained under the sufficient heat input and material flow. Therefore, the aim of this study is to investigate the weld forming ability and the weld properties by using a thickened Al alloy plate. Meanwhile, the microstructure of the Al-steel interface and the mechanical properties of the FSW joint are clarified in detail.

2. Material and methods

Cold rolled 1060Al alloy and SUS304 austenitic stainless steel plates were used as the base materials (BMs), and the chemical compositions are presented in Table 1. To investigate the influence of the thickness difference between the two BM plates on the weld forming, the thickness of the steel plates was fixed at 4.8 mm and three thickness values of 5.2 mm, 5.3 mm, and 5.5 mm were used for the 1060Al plates, respectively. The values of thickness difference (Δ) between the 1060Al plate and SUS304 steel plate were 0.4 mm, 0.5 mm, and 0.7 mm, and the related samples were defined as 0.4Δ, 0.5Δ and 0.7Δ, respectively.

In order to achieve non-contact welding between the tool and the steel, the stirring pin was completely offset into the Al side and the shoulder was not in contact with the surface of the steel plate, as shown in Fig. 1. In this study, the offset distance from the periphery of the stirring pin to the initial faying interface was 0.2 mm and the distance between the shoulder and the surface of the steel plate was zero. Therefore, for the Al plate, the plunge depth of the shoulder in the Al side was the thickness difference between these two plates. The stirring tool was made of H13 steel, and the steel and Al alloy sheets were fixed at the advancing side (AS) and retreating side (RS), respectively. The shoulder diameter of the stirring tool was 20 mm, and the diameter and length of the pin were 6 mm and 4.7 mm, respectively. The welding process was performed at a fixed rotational speed of 800 rpm and a welding speed of 50 mm/min. In order to obtain a better understanding of the joining process, the temperature histories were recorded by the K-type thermocouples placed near the interface and at the Al side 8 mm away from the interface, respectively. Prior to welding, a groove and a hole were machined in the middle of the welded plates to embed the thermocouples. The positions of the thermocouples were schematically shown in Fig. 1(b).

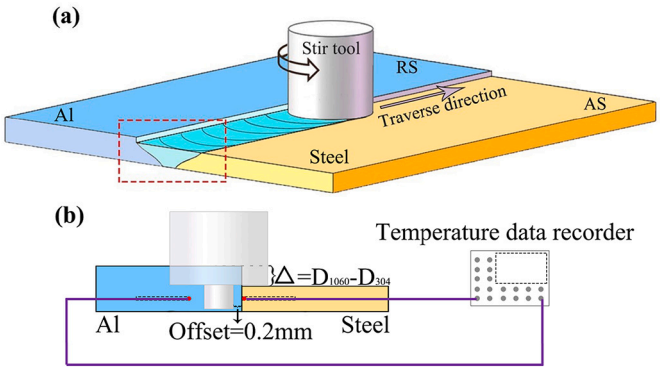

Fig. 1. Schematic diagrams of (a) FSW of 1060Al-SUS304 steel plates with different thickness (D), and (b) temperature measurement at the interface and the Al side.

After welding, the samples for microstructure observation were cut perpendicular to the welding direction and prepared by standard metallographic procedure. An optical microscope (OM, KEYENCE, VHX1000) was used to characterize the macroscopic morphology of the joints etched by Keller's reagent. The microstructure characterization of the joints was carried out using a scanning electron microscope (SEM, FEI , F50) equipped with energy dispersive spectroscopy (EDS, Oxford, INCA). Transmission electron microscopy (TEM, FEI, Talos F200C) was adopted to identify the detailed characteristics of the Al-steel interface, supplemented by the selected area electron diffraction (SAED) and EDS analysis. Thin films for TEM observation were cut parallel to the welding direction from the middle of the joint and ground to ~60 μm before being punched into 3 mm discs and further thinned by the ion-milling technique.

Vickers hardness measurement was performed along the center line on the cross-section of the joints with a load of 100 g and a dwell time of 15 s. The tensile specimens with a gauge length of 50 mm, a gauge width of 10 mm and a thickness of 4.5 mm were cut perpendicular to the weld and tensile tests were conducted at a strain rate of 10^{-3} s^{-1}.

3. Results and discussion

3.1. Macrostructure of the joints

Figs. 2(a-c) show the surface morphologies of the FSW joints. The fish-scale morphology was mostly observed on the surface of Al side and the keyholes were incomplete for the 0.4Δ and 0.5Δ joints. However, the distinct fish-scale morphology was observed on the surfaces of both Al and steel sides and a complete keyhole was also obtained at the 0.7Δ joint. In this study, the Δ value is positively correlated with the degree of the shoulder plunged into Al alloy, which indicated that more deformed Al alloy was wrapped by the shoulder at a larger Δ value. Therefore, under a large Δ value of 0.7 mm, enough Al alloy was covered on the steel surface by the forging action of the shoulder, ultimately forming a complete fish-scale morphology (Fig. 2(c)).

The cross-sectional macrographs of the FSW joints are shown in Fig. 2(d-f). There were two typical Al-steel interfaces: relatively straight interface at the 0.4Δ and 0.5Δ joints and wavy interface at the 0.7Δ

Table 1
The chemical compositions of BMs (wt%).

Alloy	Al	Fe	Cr	Ni	Si	Cu	Mn	Mg	P	N	C
1060Al	Bal	0.35	–	–	0.25	0.05	0.03	0.03	–	–	–
SUS304	–	Bal.	17.97	8	0.94	0.02	0.93	–	0.026	0.054	0.05

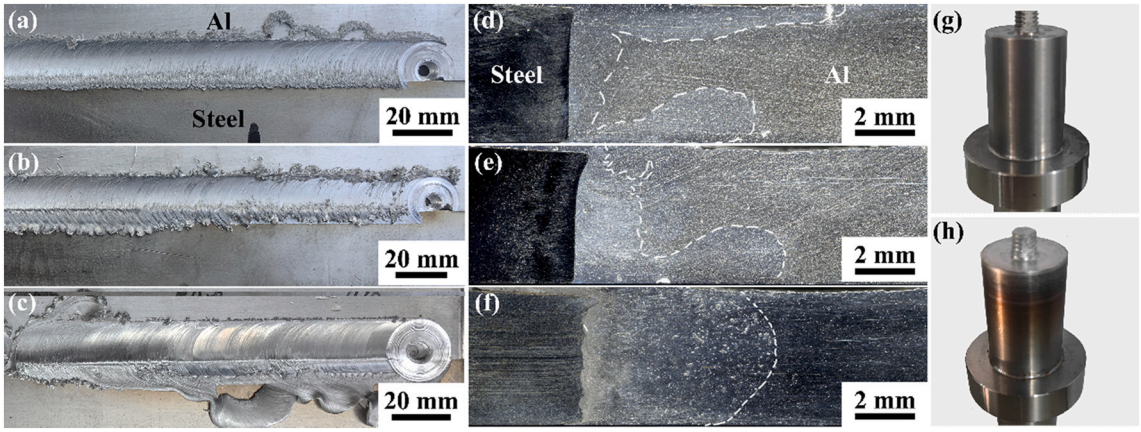

Fig. 2. Surface macrographs of (a) 0.4Δ, (b) 0.5Δ, (c) 0.7Δ joints, and the cross-sectional OM macrographs of (d) 0.4Δ, (e) 0.5Δ, (f) 0.7Δ joints, and the tool morpholgies (g) before and (h) after FSW.

joint. After etching, particle-riched areas can be observed in the nugget zones (NZs) of the three joints, which were distinguished from the adjacent area by the white dotted lines. For the 0.4Δ joint, the width of the particle-riched areas at the upper and bottom parts were larger than that in the middle part, showing a three-layered structure (Fig. 2(d)). As the Δ value increased to 0.5 mm, the particle-riched areas can only be observed at the middle and bottom parts of the NZ and the width of the middle part was about twice of that of the 0.4Δ joint (Fig. 2(e)). It is noted that a homogeneous NZ with typical onion shape was developed in the 0.7Δ joint (Fig. 2(f)). Usually, the material which differs from the matrix could be used as a marker material to track the material flow [6]. To a certain extent, the steel particles scattered in Al side can be taken as tracer materials during FSW of Al-steel. As shown by the etched morphology, the visible particle-riched area became larger with the increase of the Δ value, inferring that the material flow was enhanced in the NZ. By comparing the tool morphologies before and after FSW (Fig. 2 (g-h)), it can be noted that the shoulder and the pin were almost not worn after a weld length of about 1000 mm in the present study, which preliminarily confirmed the possibility of steel tool used in Al-steel FSW by this new method.

It is well known that the material flow is closely dependent on the welding temperature during FSW. Generally, the material subjected to plastic deformation can flow easilier at a higher temperature on account of the decreased flow stress [21]. According to the temperature histories measured both at the interface and the Al side (Fig. 3), the peak temperatures of the 0.7Δ joint were obviously higher than those of the 0.4Δ joint. A low peak temperature of <300 °C was obtained in the 0.4Δ joint, which was obviously lower than the regular welding temperature during FSW of Al alloys with sufficient material flow [22]. Therefore, insufficient material flow was achieved in the NZ due to the high flow stress at this low temperature, ruslting in the stratification of the 0.4Δ joint (Fig. 2(d)). As the Δ value increased to 0.7 mm, a high peak temperature that larger than 550 °C was obtained, and sufficient material flow were easily realized in the Al matrix of NZ according to the previous studies [22]. In this case, a homogeneous particle-riched area formed in the NZ of 0.7Δ joint, as shown in Fig. 2(f).

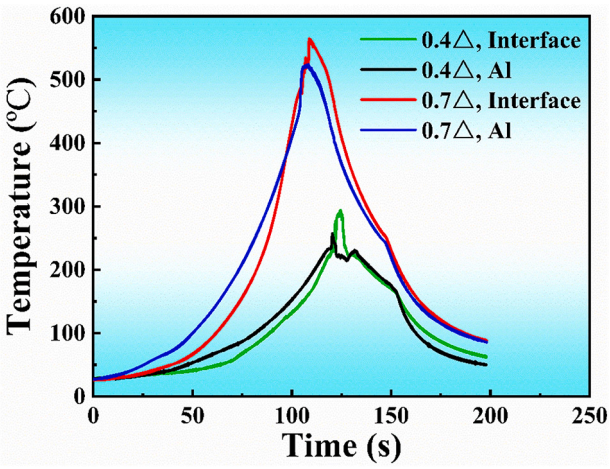

Fig. 3. Temperature histories measured at the interface and the Al side of 0.4Δ and 0.7Δ joints.

3.2. Microstructure of the joints

The cross-sectional microstructure of the FSW joints is shown in Fig. 4. It is worth pointing out that the small dispersed particles in Al matrix should be steel fragments originated from the initial steel plates rather than the tool [23]. The steel particles close to the interface were selected for further observation, and the typical morphologies are presented in Fig. 4(d-f). No IMCs were observed around the steel particle in the 0.4Δ joint while steel fragments were covered by a continuous IMCs in the 0.5Δ and 0.7Δ samples. Obviously, chemical reaction occurred easily between Al matrix and the scattered steel particles at the relatively high Δ values, due to the high temperature and enhanced material flow.

Figs. 4(g-i) show the magnified images of the Al-steel interfaces as marked by the red rectangles in Figs. 4(a-c). As revealed, cracks were visible at the interfaces of 0.4Δ and 0.5Δ joints whereas the interface of the 0.7Δ joint was free of crack defects. The difference of the interfaces in the three joints can be well elucidated by the temperature histories shown in Fig. 3. One of the remarkable features of welding process is that the weld temperature changes very quickly and the reaction time between Al and steel is rather short. Therefore, sufficient heat input is required to ensure an effective metallurgical bonding of Al to steel. The heat input at the interface of 0.4Δ joint was insufficient in limited time compared with that of the 0.7Δ joint, resulting in obvious crack defects (Fig. 4(g)). On the other hand, Al—Fe IMCs, which were frequently found at the Al-steel interface, could not be clearly observed at the interface of 0.7Δ joint (Fig. 4(i)), implying that extremely thin IMCs might be formed.

3.3. Characterization of Al-steel interface

To further characterize the interface structure of the reaction layer, TEM analysis was carried out on the 0.7Δ sample, as illustrated in Fig. 5. Fig. 5(a) displays the scanning TEM (STEM) image taken at the interface. A distinct interface existed between Al and steel on account of the

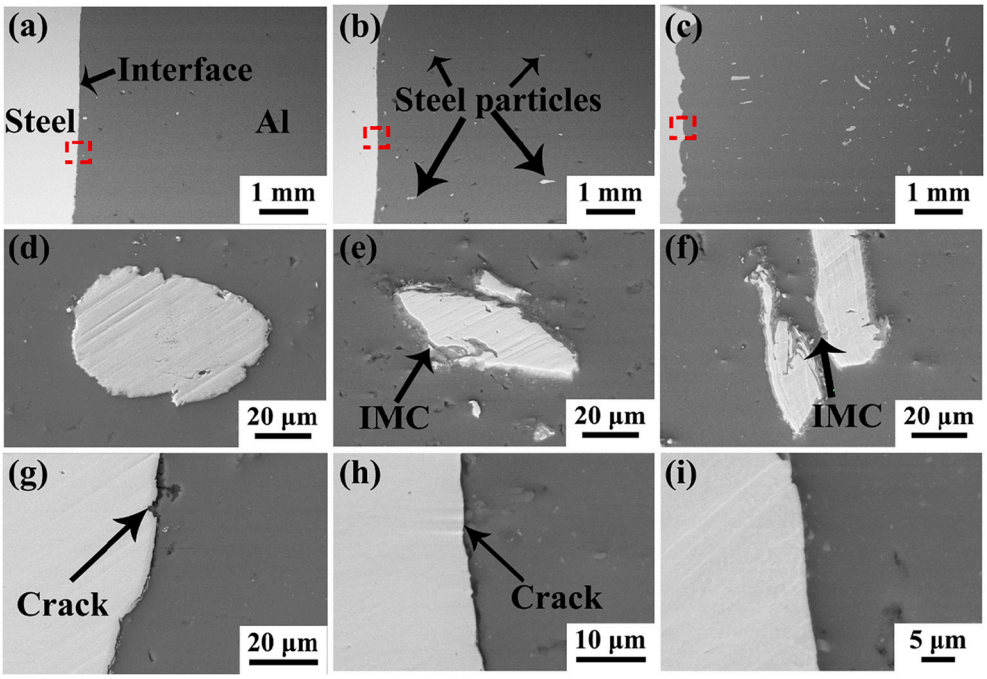

Fig. 4. SEM backscattered-electron images of (a) 0.4Δ, (b) 0.5Δ, (c) 0.7Δ joints, magnified images of particles in (d) 0.4Δ, (e) 0.5Δ, (f) 0.7Δ joints, and interfaces in (g) 0.4Δ, (h) 0.5Δ, (i) 0.7Δ joints.

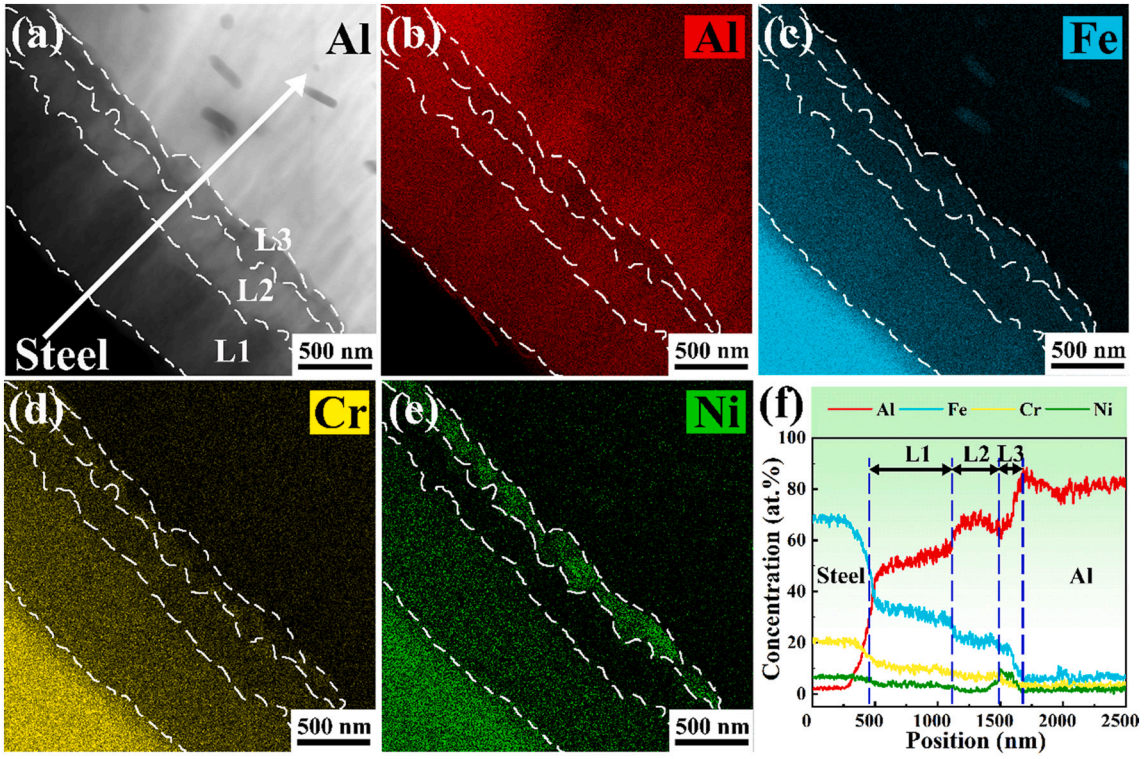

Fig. 5. (a) STEM image taken at the interface of 0.7Δ joint, (b-e) corresponding elemental mappings at the interface, (f) EDS line scanning result along the white line in (a).

different element contents, which can be divided into three layers: L1 layer (~600 nm thickness), L2 layer (~250 nm thickness) and L3 layer (~100 nm thickness). Different from this observation, Lee et.al [24] observed ~4 μm mixed layer at the interface region of Al-steel FSW joint besides the IMC layers. Submicron stacked structure was easily produced in the mixed layer under intense plastic deformation happened at the steel side owing to contact between the tool and steel plate. Nevertheless, such stacked structure disappeared using the method with no contacting between the tool and the steel plate.

Figs. 5(b-e) show the corresponding element distribution mappings taken from Fig. 5(a), including Al, Fe, Cr and Ni. Meanwhile, the EDS line analysis along the white line in Fig. 5(a) is presented in Fig. 5(f). It is

clear that three obvious layers were characterized by the element analysis, which was consistent with the STEM microstructure. The contents of Fe and Cr elements decreased gradually while the content of Al incresed from steel side to Al side, which was a regular phenomenon in a diffusion reaction controlled Al-steel interface [25,26]. However, an obvious segregation of Ni element was observed in L3 layer while a relatively poor Ni area was found in L2 layer simultaneously (Fig. 5(e)).

Generally, the difference in element distribution is related to the variation in their diffusion coefficient, and diffusion in metals depends strongly on temperature. The diffusion rates of Fe, Cr, and Ni at the temperature range of 327 °C to 660 °C have been summarized in Refs [27], where the diffusion rate of Ni is from 9.58×10^{-17} m^2 s^{-1} to 3.12×10^{-12} m^2 s^{-1}, the diffusion rate of Fe is from 3.98×10^{-45} m^2 s^{-1} to 3.43×10^{-13} m^2 s^{-1} and the diffusion rate of Cr is from 6.85×10^{-55} m^2 s^{-1} to 1.69×10^{-15} $m^2 s^{-1}$ in Al matrix. In this study, the peak temperature of the interface during the welding process was measured as 564 °C (Fig. 3), satisfying the above temperature range. That is why Ni atoms were favored for enrichment in L3 layer in comparison to Fe and Cr atoms. Besides, it is also reported that Fe atom tends to occupy the position of Ni atom during the diffusion process [28,29]. Therefore, the concentration of Ni atom is low in the L2 and L3 layers.

SAED was used to determine the crystal structure of the phases in L1, L2 and L3 layers, as shown in Fig. 6. The diffraction ring patterns in Figs. 6(a-b) reveal that nanometer-scale particles existed in L1 and L2 layers. By analyzing the d-spacing from different sets of planes, the phases of IMCs in L1 layer and L2 layer were confirmed to be Al_5Fe_2 and $Al_{13}Fe_4$ phase, respectively. As for L3 layer, the diffraction spots shown in Fig. 6(c) indicated that this layer was mainly composed of Al, although enrichment of Ni atoms existed. It can be proved that an Al-based solid solution was formed in L3 layer instead of the IMC layer according to the combination of the structure and composition analysis.

3.4. Mechanical properties

The microhardness distributions of FSW joints are illustrated in Fig. 7 (a). It can be seen that the hardness values of the heat affect zone (HAZ) in Al side were slightly lower than that of the Al BM, which can be attributed to annealing effect in the cold rolled Al alloy. Previous investigations showed that abnormally fluctuating distribution of hardness values was found in the NZ, and some hardness values was even higher than that of the steel BM due to a considerable amount of scattered steel fragments and IMCs [30,31]. Differently, the hardness values were almost the same in the NZ of the FSW joints in this study. Further, the hardness values in NZ were still lower than that of Al BM although the grain sizes decreased owing to the recrystallization process during FSW. Obviously, the number of the steel particles and IMCs was greatly reduced in the NZ compared to that of the conventional Al-steel FSW joints.

Fig. 7(b) shows the engineering stress-strain curves of the FSW joints. The tensile strength was generally low for the 0.4Δ and 0.5Δ joints and the fracture occurred along the interface, which was attributed to the cracks at the interface. However, the tensile strength of the 0.7Δ joint can reach to 104 MPa (about 95% of 1060Al BM) and the fracture occurred in the HAZ of Al side, indicating that an excellent metallurgical bonding was achieved at the interface of Al-steel joint. As mentioned before, sufficient heat input and material flowability were achieved at a higher Δ value, facilitating the bonding between Al and steel.

The stable Al—Fe IMCs in the Al—Fe phase diagram usually consist of Al-rich ($Al_{13}Fe_4$, Al_5Fe_2, Al_2Fe, Al_3Fe_2, and AlFe) and Fe-rich ($AlFe_3$) IMCs. Based on the first-neighbor hopping mechanism, it was revealed that penetration of Fe into Al was much deeper than that from Al to Fe [32]. Besides, the diffusion coefficient of Fe into Al is larger than that of Al into Fe, the reaction kinetics of Al—Fe IMCs is controlled by the diffusion of Fe [33]. Hence, the formation of Al-rich IMCs are easier than that of Fe-rich IMCs at the interface. Moreover, the Gibb's free energy values of Al_5Fe_2 and $Al_{13}Fe_4$ are lower than the other three Al-rich IMCs [34]. Therefore, the Al_5Fe_2 and $Al_{13}Fe_4$ are prone to spontaneously form at the Al—Fe interface during the welding process, which was consistent with the outcomes of Fig. 5 and Fig. 6.

However, due to the intrinsic brittleness of IMCs, Al_5Fe_2 and $Al_{13}Fe_4$ both tend to exhibit high hardness and low toughness. The increase in the thickness of such IMCs gives rise to crack susceptibility, which leads to the early fracture in the IMC layers and decreases the mechanical properties of the joints. Therefore, it is well accepted that the thinner IMCs are more favorable for the mechanical properties of the joints [5]. Meanwhile, the grain refinement of IMCs at the interface can improve the Al-steel joint strength [35]. Combining the interface microstructure (Fig.5(a)) and tensile strength (Fig.7(b)), the excellent metallurgical bonding between Al and steel was facilitated with the nanoscaled $Al_{13}Fe_4$ and Al_5Fe_2 IMCs at the interface (total thickness of IMCs <1 μm) in the current study.

It can be seen from the above results that as long as the Al alloy and steel plates are designed with an appropriate thickness difference, high-quality joint can be obtained even if the tool does not contact with the steel plate. The thickened Al alloy guarantees the sufficient heat input and material flow during FSW, resulting in the excellent metallurgical bonding at the Al-steel interface. On the other hand, only small amount of steel particles and IMCs formed in the NZ during FSW, and the material flow can be similar to that of the Al alloy. In this case, steady welding can be realized in a long-distance FSW of Al to steel, which is very important in the industrial application. In a word, this study provides a new and effective method with low cost and high quality in FSW of Al alloy to high fusion-point metals.

4. Conclusion

In this study, high-quality 1060Al-SUS304 steel joint was successfully obtained by FSW with no contacting between the tool and the steel plate, and the ordinary H13 steel tool was used under the condition that the Al alloy plates were thickened. The effects of different Δ values on the microstructure and the mechanical properties of the FSW joints were studied in detail. The main conclusions can be summarized as follows:

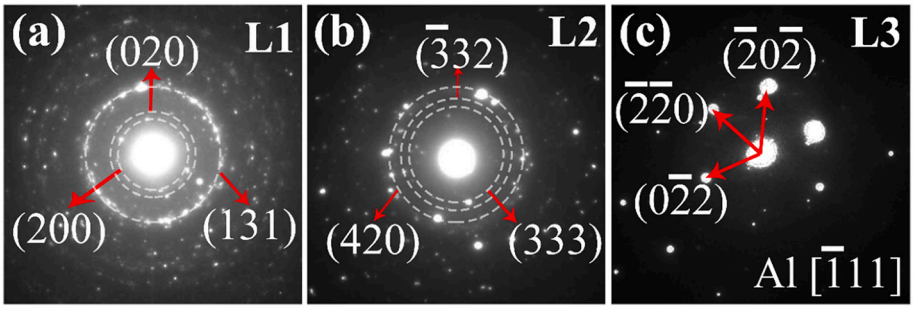

Fig. 6. SAED patterns taken from (a) L1 layer, (b) L2 layer and (c) L3 layer.

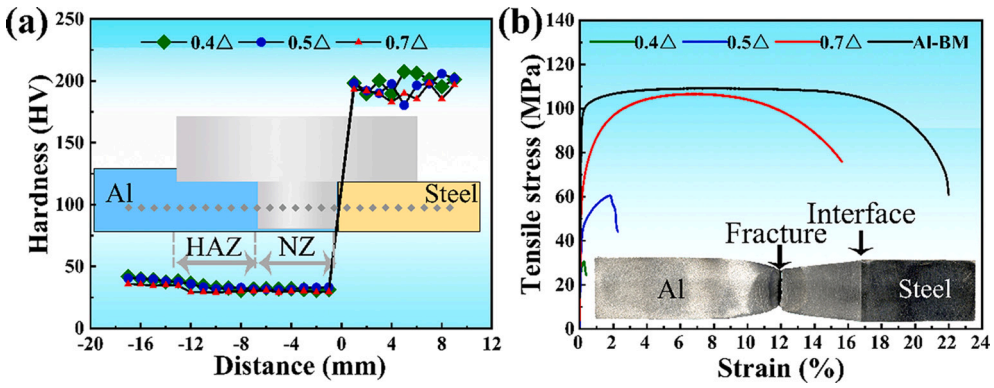

Fig. 7. (a) Microhardness distribution along the cross-section of FSW joints and (b) the engineering stress-strain curves of FSW joints and Al BM.

(1) When the Δ value increased from 0.4 mm to 0.7 mm, the fish-scale morphology and the keyhole became complete. The distribution of scattered steel particles was homogeneous in the NZ of the 0.7Δ joint due to sufficient material flow.
(2) Fracture happened at the interface during welding of 0.4Δ and 0.5Δ joints while the joint without defects was obtained at a larger Δ value of 0.7 mm owing to the sufficient heat input.
(3) The interfacial structure of 0.7Δ joint was divided into three layers: Al_5Fe_2 and $Al_{13}Fe_4$ IMC layers near steel side, and Al-based solid solution layer near Al side.
(4) The tensile strength of the 0.7Δ joint was as high as 104 MPa, reaching 95% of that of 1060Al BM, indicating that an excellent metallurgical bonding was obtained at the Al-steel interface.

Declaration of Competing Interest

We declare that we have no known competing financial interests or personal relationships that could influence the work in this paper.

Data availability

Data will be made available on request.

Acknowledgments

The author M. Zhang is grateful to Dr. J. Cai for her excellent experimental assistance. This work was supported by the National Natural Science Foundation of China under Grant Nos. 51901225 and 52034005, the Liaoning Province Excellent Youth Foundation (2021-YQ-01), and the Youth Innovation Promotion Association of the Chinese Academy of Sciences (Y2021061).

References

[1] Y.Q. Liu, R.L. Liu, B. Liu, Z.T. Zhu, Y.X. Li, H. Chen, Interface characterization and tensile performance of deep-penetration welding-brazing of thick aluminium/steel butt joints, Mater. Charact. 186 (2022), 111811.
[2] F.C. Liu, P. Dong, J. Zhang, W. Lu, A. Taub, K. Sun, Alloy amorphization through nanoscale shear localization at Al-Fe interface, Mater. Today Phys. 15 (2020), 100252.
[3] T. Yang, W. Dai, L. Chen, Y. Zhuang, Z. Zhou, J. Hu, Thermodynamically revealing the effect mechanism of cu on the interfacial metallurgical reaction for Al/steel welding-brazing joint, J. Mater. Process. Technol. 299 (2022), 117372.
[4] L. Cui, D.Q. Lu, D.Y. He, F. Pan, Hybrid laser-metal inert gas keyhole welding of thick steel/Al butt joints, J. Laser Appl. 31 (2019) 1–9.
[5] J. Yang, J.P. Oliveira, Y. Li, C. Tan, C. Gao, Y. Zhao, Z. Yu, Laser techniques for dissimilar joining of aluminum alloys to steels: a critical review, J. Mater. Process. Technol. 301 (2022), 117443.
[6] R.S. Mishra, Z.Y. Ma, Friction stir welding and processing, Mater. Sci. Eng. R 50 (2005) 1–78.
[7] R. Jabraeili, H.R. Jafarian, R. Khajeh, N. Park, Y. Kim, A. Heidarzadeh, A.R. Eivani, Effect of FSW process parameters on microstructure and mechanical properties of the dissimilar AA2024 Al alloy and 304 stainless steel joints, Mater. Sci. Eng. A 814 (2021), 140981.
[8] A. Kar, B. Vicharapu, Y. Morisada, H. Fujii, Elucidation of interfacial microstructure and properties in friction stir lap welding of aluminium alloy and mild steel, Mater. Charact. 168 (2020), 110572.
[9] S.H.C. Park, Y.S. Sato, H. Kokawa, K. Okamoto, S. Hirano, M. Inagaki, Boride formation induced by PCBN tool wear in friction-stir-welded stainless steels, Metall. Mater. Trans. A. 40 (3) (2009) 625–636.
[10] L.H. Wu, D. Wang, B.L. Xiao, Z.Y. Ma, Tool wear and its effect on microstructure and properties of friction stir processed Ti–6Al–4V, Mater. Chem. Phys. 146 (3) (2014) 512–522.
[11] Z. Iqbal, N. Saheb, A.R. Shuaib, W-25%re-HfC composite materials for pin tool material applications: synthesis and consolidation, J. Alloys Compd. 674 (2016) 189–199.
[12] N. Karimi, S. Nourouzi, M. Shakeri, M. Habibnia, A. Dehghani, Effect of tool material and offset on friction stir welding of Al alloy to carbon steel, Adv. Mater. Res. 445 (2012) 747–752.
[13] M. Habibnia, M. Shakeri, S. Nourouzi, M.K.B. Givi, Microstructural and mechanical properties of friction stir welded 5050 Al alloy and 304 stainless steel plates, Int. J. Adv. Manuf. Technol. 76 (2015) 819–829.
[14] R. Rai, A. De, H.K.D.H. Bhadeshia, T. DebRoy, Review: friction stir welding tools, Sci. Technol. Weld. Join. 16 (2013) 325–342.
[15] T. Watanabe, H. Takayama, A. Yanagisawa, Joining of aluminum alloy to steel by friction stir welding, J. Mater. Process. Technol. 178 (2006) 342–349.
[16] K.K. Ramachandran, N. Murugan, S.S. Kumar, Effect of tool axis offset and geometry of tool pin profile on the characteristics of friction stir welded dissimilar joints of aluminum alloy AA5052 and HSLA steel, Mater. Sci. Eng. A 639 (2015) 219–233.
[17] N. Karimi, M. Shakeri, M. Habibnia, S. Nourouzi, Joining of 1100 Al alloy to AISI 1045 carbon steel by friction stir welding, Appl. Mech. Mater. 152-154 (2012) 418–423.
[18] Z. Shen, Y. Chen, M. Haghshenas, A.P. Gerlich, Role of welding parameters on interfacial bonding in dissimilar steel/aluminum friction stir welds, Eng. Sci. Technol. Intern. J. 18 (2) (2015) 270–277.
[19] Z. Shen, J. Chen, Y. Ding, J. Hou, B.S. Amirkhiz, K. Chan, A.P. Gerlich, Role of interfacial reaction on the mechanical performance of Al/steel dissimilar refill friction stir spot welds, Sci. Technol. Weld. Join. 23 (6) (2018) 462–477.
[20] Z. Shen, Y. Ding, J. Chen, B.S. Amirkhiz, J.Z. Wen, L. Fu, A.P. Gerlich, Interfacial bonding mechanism in Al/coated steel dissimilar refillfriction stir spot welds, J. Mater. Sci. Technol. 35 (6) (2019) 1027–1038.
[21] J.M. Piccini, H.G. Svoboda, Tool geometry optimization in friction stir spot welding of Al-steel joints, J. Manuf. Process. 26 (2017) 142–154.
[22] T. Nakamura, T. Obikawa, I. Nishizaki, M. Enomoto, Z. Fang, Friction stir welding of non-heat-treatable high-strength alloy 5083-O, Metals. 8 (4) (2018).
[23] M. Dehghani, A. Amadeh, S. Mousavi, Investigations on the effects of friction stir welding parameters on intermetallic and defect formation in joining aluminum alloy to mild steel, Mater. Des. 49 (2013) 433–441.
[24] W.B. Lee, M. Schmuecker, U.A. Mercardo, G. Biallas, S.B. Jung, Interfacial reaction in steel-aluminum joints made by friction stir welding, Scr. Mater. 55 (2006) 355–358.
[25] B. Murugan, G. Thirunavukarasu, S. Kundu, S. Kailas, S. Chatterjee, Interfacial microstructure and mechanical properties of friction stir welded joints of commercially pure aluminum and 304 stainless steel, J. Mater. Eng. Perform. 27 (6) (2018) 2921–2931.
[26] H. Ma, G. Qin, Z. Dang, P. Geng, Interfacial microstructure and property of 6061 aluminium alloy/stainless steel hybrid inertia friction welded joint with different steel surface roughness, Mater. Charact. 179 (2021), 111347.
[27] H.N. Yao, H.Y. Wen, K. Chen, M.Y. Jiang, K.M. Reddy, K. Kondoh, M. Wang, X. M. Hua, A.D. Shan, Interfacial phases formed in friction stir lap welding high entropy alloy to Al alloy, Scr. Mater. 201 (2021) 1–4.
[28] C.L. Fu, J. Zou, Site preference of temary alloying additions in FeAl and NiAl by first - principles calculations, Acta Mater. 44 (4) (1996) 8.
[29] L. Eleno, K. Frisk, A. Schneider, Assessment of the Fe–Ni–Al system, Intermetallics 14 (10–11) (2006) 1276–1290.
[30] H.A. Derazkola, F. Khodabakhshi, Intermetallic compounds (IMCs) formation during dissimilar friction-stir welding of AA5005 aluminum alloy to St-52 steel:

numerical modeling and experimental study, Int. J. Adv. Manuf. Technol. 100 (2019) 2401–2422.
[31] S.Y. Anaman, H.H. Cho, H. Das, J.S. Lee, S.T. Hong, Microstructure and mechanical/electrochemical properties of friction stir butt welded joint of dissimilar aluminum and steel alloys, Mater. Charact. 154 (2019) 67–79.
[32] J. Syarif, K. Badawy, H.A. Hussien, Atomistic simulation of the diffusion behavior in Al-Fe, Nucl. Mater. Energy. 29 (2021), 101073.
[33] G.Q. Wang, Y.Q. Wang, R.H. Duan, G.M. Xie, Enhancements in the bonding properties of a friction stir lap-welded interstitial free steel and Al alloy by introducing a Ni interlayer, Metals 11 (11) (2021).
[34] T. Sapanathan, I. Sabirov, P. Xia, M.A. Monclus, J.M. Molina-Aldareguia, P. J. Jacques, A. Simar, High temperature in situ SEM assessment followed by ex situ AFM and EBSD investigation of the nucleation and early growth stages of Fe-Al intermetallics, Scr. Mater. 200 (2021), 113910.
[35] R. Beygi, R.J.C. Carbas, A.Q. Barbosa, E.A.S. Marques, L.F.M. da Silva, A comprehensive analysis of a pseudo-brittle fracture at the interface of intermetallic of η and steel in aluminum/steel joints made by FSW: microstructure and fracture behavior, Mater. Sci. Eng. A 824 (2021), 141812.